Reprinted from Advanced Ceramic Materials, Vol. 3, No. 1, January 1988

Superplasticity of TZP/Al_2O_3 Composite

FUMIHIRO WAKAI*
Ceramic Science Dept., Government Industrial Research Institute, Nagoya, 462 Japan

HIDEZUMI KATO
Research & Development Center, Suzuki Motor Co. Ltd., Hamamatsu, 432-91 Japan

The superplastic behavior of the composite Y-TZP/Al_2O_3 (20 wt%) in uniaxial tension has been evaluated. Large elongation (>200%) indicated superplasticity. The stress exponent and activation energy of the composite were found to be the same order with those of Y-TZP. The flow behavior of the composite containing Al_2O_3 grains could be described by a rheological model as a non-Newtonian flow modified by the second-phase grains. The cavitation damage and the creep crack growth could be reduced by keeping the strain rate low enough that a specimen elongated 100% at elevated temperature maintained a strength of 1800 MPa at room temperature.

Superplasticity is a mode of deformation that can be observed in polycrystalline materials that have an ultrafine grain size and equiaxed grain shape.[1] Phenomenologically it is defined as the ability to exhibit extraordinary elongation during tensile deformation. The essential characteristic for "structural" or "micrograin" superplasticity is the microstructural stability during deformation, i.e. the stability of grain size and shape and the suppression of cavity nucleation and growth.

Superplasticity in ceramics has not been found, except for β-spodumene glass-ceramics,[2] because of the propensity for cavity growth or creep crack growth during the deformation under tensile stress and resulting fracture before the achievement of large plastic strains.[3,4] There has been confusion in the use of terms for superplasticity of ceramics, because the term "structural superplasticity" often has been used to describe high ductility of fine-grained ceramics during compressive deformation.[5] The specific stress distribution in compression or superposition of a hydrostatic pressure prevents cavitation and improves ductility.[6] However, this behavior does not necessarily indicate that superplastic elongation will occur in tensile loading.

Previous work has shown superplasticity in Y_2O_3-stabilized tetragonal ZrO_2 polycrystals (Y-TZP) in the temperature range of a two-phase field of tetragonal (t)-cubic (c) mixtures in the ZrO_2-Y_2O_3 system.[7-10] The superplasticity of submicrometer grain size Y-TZP occurs primarily by the grain-boundary sliding. It is believed that the coexistence of tetragonal and cubic phase under testing conditions contributes to the stability of the grain size,[8,11] thereby enhancing further deformation.

Grain growth will also be retarded by the presence of the second-phase grains in various ZrO_2-toughened ceramics (ZTC) that are two-phase composites.[12-14] Kellet and Lange[13] studied forging characteristics of fine-grained Al_2O_3/ZrO_2 composites containing 20 vol% ZrO_2 and achieved compressional strains of 80% without tearing. Wakai *et al.*[15] observed extraordinarily large deformation (true strain of -1.8) of TZP/Al_2O_3 composites containing 20 wt% Al_2O_3 in compression testing. The superplasticity of TZP/Al_2O_3 was predicted because there were many similarities between the compressive deformation behavior of superplastic Y-TZP and that of the composite.

In this report, the superplastic deformation of TZP/Al_2O_3 was studied by uniaxial tension tests and tensile creep tests. Flow behavior of the composite was analyzed from a rheological viewpoint, and the fracture of superplastic material was also studied to determine a way to minimize and control the cavitation damage.

EXPERIMENTAL PROCEDURE

SPECIMEN PREPARATION

The Y-TZP/Al_2O_3 composite*[16,17] was fabricated from submicrometer composite powder (80 wt% ZrO_2 containing 3 mol% Y_2O_3 and 20 wt% Al_2O_3). The powder was pressed into rectangular platelike forms at 49 MPa and then isostatically cold-pressed at 196 MPa. The green compacts were sintered at 1400°C and then isostatically hot-pressed at 1500°C and 98 MPa for 2 h in Ar gas. The average grain size was $\approx$0.5 μm for both ZrO_2 and Al_2O_3. The density and the 4-point bend strength at room temperature were 5.49 g/cm^3 and 1880 MPa, respectively.

Three types of specimens were prepared for tension tests and tensile creep tests. A tension specimen had a gage length of either 30 or 16 mm and a circular cross section of $\approx$3 mm in diameter (Fig. 1). Specimens used in tensile creep tests[7] were designed to have "targets" on both sides of the gage length portion (30 mm) so that the creep strain could be measured using a noncontacting electro-optical extensometer. All specimens were diamond-machined from isostatically hot-pressed plates (15 by 80 by 4 mm).

TESTING PROCEDURE

Tension tests at constant cross-head speeds were conducted using a universal testing machine.† The specimen was heated to the test temperature (up to 1500°C) in air by using a $MoSi_2$-element furnace with a temperature variation of $\pm$5°C over a length of 50 mm. Displacement of cross-head was measured and calibrated

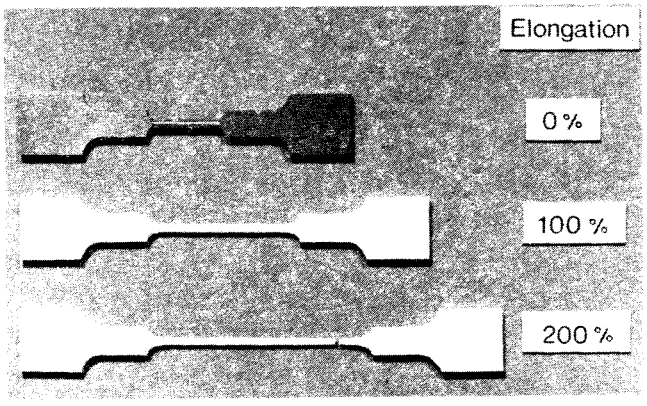

Fig. 1. Tensile specimens of TZP/Al_2O_3 composite showing superplastic elongation.

*Member, the American Ceramic Society.
*Toyo Soda Manufacturing Co. Ltd., Kanagawa, Japan.
†Instron Corp., Canton, MA.

Received November 12, 1986; revised copy received June 10, 1987; approved June 12, 1987.

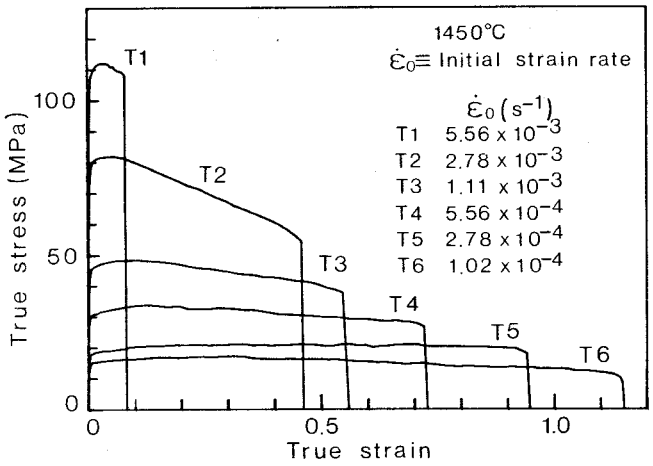

Fig. 2. True stress as a function of true strain for a constant cross-head speed at 1450°C.

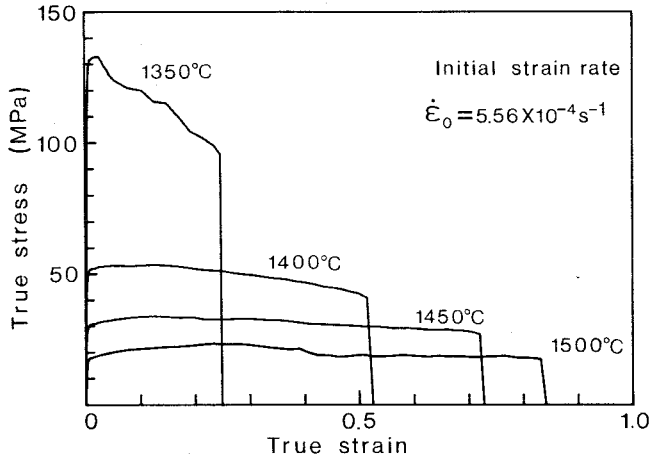

Fig. 4. True stress as a function of true strain for different temperatures at an initial strain of 5.56 × 10^{-4} s^{-1}.

to the elongation against the gage-length portion of the specimen. Tensile creep tests at constant loads were performed in air using an apparatus[18] with an electro-optical extensometer.‡ The grips, which were originally designed by Oji *et al.*,[19] were made from SiC. In essence, the shoulder portion of specimen was put between two SiC pins that were retained by the grip connected to a universal joint. The relation between stress and strain rate was obtained by rapidly changing the testing stresses.

The strength of deformed specimens was measured by 4-point bending (lower span 30 mm and upper span 20 mm) at room temperature. Bend specimens were cut from the gage-length portion of superplastically elongated specimens. The density of deformed specimens was measured by the Archimedes method. The microstructures of as-sintered and deformed specimens were observed by scanning electron microscopy (SEM) on the polished and thermally etched surfaces. The longitudinal ($d_{//}$) and transverse ($d_{\perp}$) dimensions of the elongated grains were measured in sections taken parallel to the tensile direction.

DATA ANALYSIS

True strain (ε_t) is defined as:

$$\varepsilon_t = \ln (l/l_0) \tag{1}$$

where l and l_0 are the elongated and the original gage length, respectively. By assuming that there is no local necking, true stress (σ_t) can be calculated by the following relation:

$$\sigma_t = S \exp (\varepsilon_t) \tag{2}$$

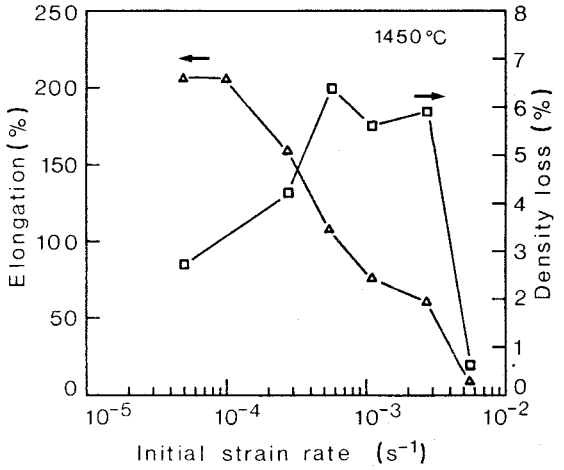

Fig. 3. Elongation to failure versus initial strain rate at 1450°C.

where S is nominal stress ($S = P/A_0$, P is applied load and A_0 is cross section of the original specimen).

RESULTS

TENSILE ELONGATION

The TZP/Al_2O_3 composite showed large superplastic elongations (up to 200%) in uniaxial tension tests (Fig. 1). The dark composite turned white after heating in air. The appearance of a deformed specimen (100%) was characterized by the lack of a necked region. Unstable deformation occurred just before the fracture, so slight tapering of gage length portion was observed in the 200% elongated and fractured specimen.

The true stress-true strain curves (Fig. 2) were calculated from the load-displacement curves obtained at a constant cross-head speed under the assumption of a uniform deformation. Flow softening (i.e. the negative slope in flow curve)[20] was clearly observed at higher initial strain rates. The degree of flow softening decreased with the reduction of initial strain rate, and the deformation proceeded under constant flow stresses at lower strain rates. The steady reduction of true stress occurs partly because of the reduction of effective strain rate during deformation. However, it is believed that the rapid strain softening observed at higher strain rates in Fig. 2 was not an apparent one but was due to cavitation or creep crack growth during deformation.

In the case in which initial strain rates were higher than 10^{-3} s^{-1}, the peak stress appeared at nominal strains of ≈3 to 8%. The peak in flow curves became indistinct at lower strain rates and the strain at peak increased. In the flow curves that showed a peak stress, flow hardening (i.e. positive slope in flow curve) occurred at the beginning of deformation with later slight flow softening.

The elongation to failure was strongly affected by strain rate with larger elongation possible at lower strain rates (Fig. 3). Elongation >200% was obtained at an initial strain rate of 1.02 × 10^{-4} s^{-1} at 1450°C. A further increase in the elongation was not observed at even lower strain rates. The density loss of elongated specimens was also plotted in Fig. 3. The maximum density loss was observed for specimens elongated at intermediate strain rates. It indicated that the density loss was a complicated function of both strain rate and total elongation.

The true stress-true strain curves at an initial strain rate of 5.56 × 10^{-4} s^{-1} at different temperatures are shown in Fig. 4. For temperatures >1400°C, the specimens deformed at constant flow stress and elongation at failure increased with increasing temperature. Strain softening was observed at 1350°C and the specimen fractured at small elongation. Semibrittle fracture occurred for

‡DDM1000, Zimmer Co., FRG.

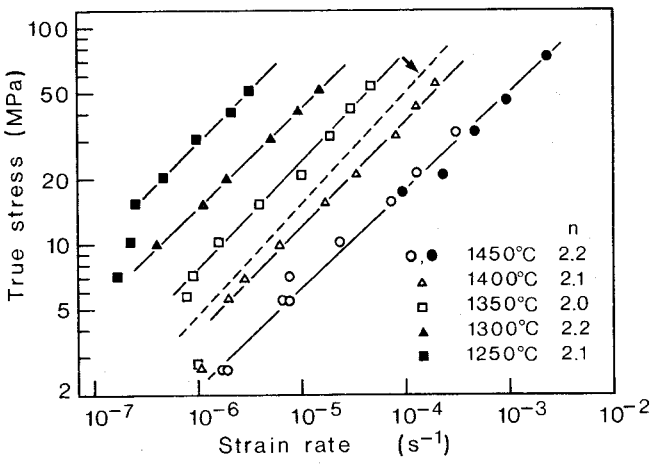

Fig. 5. Flow stress as a function of strain rate.

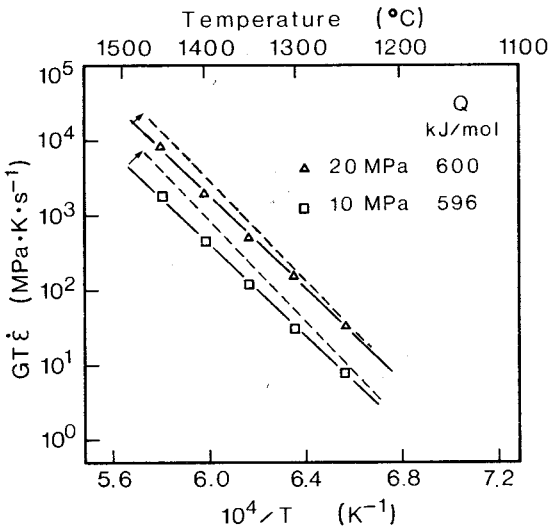

Fig. 6. Temperature-compensated strain rate at constant stress versus the reciprocal of absolute temperature.

the specimen deformed at 5.56×10^{-4} s^{-1} and 1300°C, although creep deformation at the same temperature was possible when strain rate was lower than 1×10^{-5} s^{-1}.

FLOW BEHAVIOR

The strain rate, $\dot{\varepsilon}$, in superplasticity may be expressed by the Dorn equation for a diffusion-controlled process:[21]

$$\dot{\varepsilon} = \frac{AGb}{kT}\left(\frac{b}{d}\right)^p\left(\frac{\sigma}{G}\right)^n D_0 \exp\left(-Q/RT\right) \quad (3)$$

where G is shear modulus, b is Burger's vector, k is Boltzmann's constant, T is absolute temperature, d is grain size, σ is stress, D_0 is a frequency factor, Q is the activation energy, R is a gas constant, A is a dimensionless constant, and n and p are exponents of stress and inverse grain size, respectively.

The relation between flow stress and strain rate obtained by creep tests at a constant load is plotted on a logarithmic scale in Fig. 5. Additional experimental points (full circles), corresponding to the stress value obtained at a true strain of 0.1 from flow curves in Fig. 2, have also been plotted. The stress exponent was calculated from the slope of lines in Fig. 5. The plot yielded $n = 2.1 \pm 0.1$ at the strain rates from 10^{-2} to 10^{-7} s^{-1} in the temperature range from 1250° to 1450°C.

The strain rates at 10 and 20 MPa were determined from Fig. 5 and the data are plotted in the form of ln $(GT\dot{\varepsilon})$ vs $1/T$ (Fig. 6). The shear modulus of Y-TZP at elevated temperatures measured by a resonance method was used in the calculation of the temperature-compensated strain rate for the composite. Using these values, an activation energy of 596 and 600 kJ/mol was calculated for 10 and 20 MPa loading, respectively. The flow behavior of TZP/Al_2O_3 (20 wt%) composite showed fairly good agreement with the tensile creep results of Y-TZP ($n = 2$, $Q = 600 \pm 60$ kJ/mol.)[8]

MICROSTRUCTURAL OBSERVATION

Changes in the microstructure before and after the superplastic deformation is shown in Fig. 7. The microstructural observation was conducted on the polished and thermally etched surfaces. The as-sintered specimen contained equiaxed Al_2O_3 grains dispersed among equiaxed ZrO_2 matrix grains. At an elongation of 100%, each grain was elongated slightly in the tensile direction and showed an anisotropic linear orientation. The elongated grains in the deformed specimens are characterized by the ratio of longitudinal ($d_{//}$) to transverse ($d_\perp$) dimensions of the grains, i.e. the grain aspect ratio (GAR). Figure 7(*B*) and (*C*) illustrate the microstructure of specimens deformed 100% at 1450°C. The GAR of ZrO_2 grains was 1.15, and the GAR of Al_2O_3 grains in specimens deformed at 5.56×10^{-4} s^{-1} (Fig. 7(*B*)) and at 5.56×10^{-5} s^{-1} (Fig. 7(*C*)) was 1.5 and 1.3, respectively. When the total strain (ε_{tot}) is expressed as a sum of the intragranular strain (ε_g), which can be calculated from GAR,[15] and the strain ascribed to the grain-boundary sliding (ε_{gbs}), the contribution of ε_{gbs} to ε_{tot} is estimated to be 60 to 80%.

Flow stress of the composite was 30 MPa at 5.56×10^{-4} s^{-1} and at 1450°C. Under this stress, Al_2O_3 grains could deform by an intragranular mechanism, basal slip, because the flow stress of basal slip was ≈30 MPa at 4×10^{-5} s^{-1}.[22] Basal crystallographic texture in deformed Al_2O_3/ZrO_3 composite containing 20 vol% ZrO_2 was observed by Kellett and Lange.[14] On the other hand, flow stress of Y_2O_3-stabilized ZrO_2 single-crystal was 150 MPa at 1.3×10^{-5} s^{-1} at 1400°C.[23] So, intragranular strain of ZrO_2 grain was smaller than that of Al_2O_3.

Grain growth was clearly observed during deformation (Fig. 7(*B*) and (*C*)). The strain-enhanced grain growth during su-

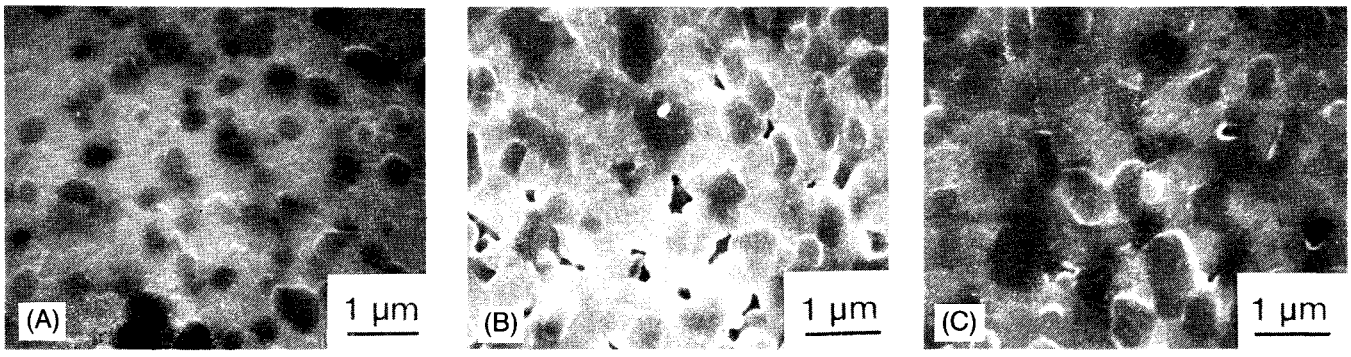

Fig. 7. (*A*) SEM micrograph of the as-sintered composite; Al_2O_3 is seen as a dark phase, (*B*) after 100% elongation at $\dot{\varepsilon}_0 = 5.56 \times 10^{-4}$ s^{-1} and 1450°C (tension axis is vertical), and (*C*) after 100% elongation at $\dot{\varepsilon}_0 = 5.56 \times 10^{-5}$ s^{-1} and 1450°C (tension axis is vertical).

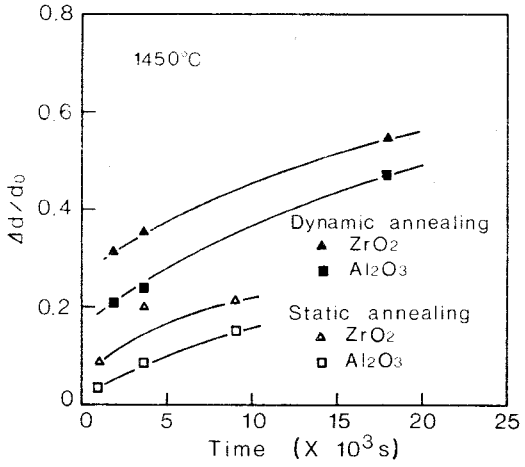

Fig. 8. Grain growth during dynamic and static annealing of TZP/Al_2O_3 composite at 1450°C.

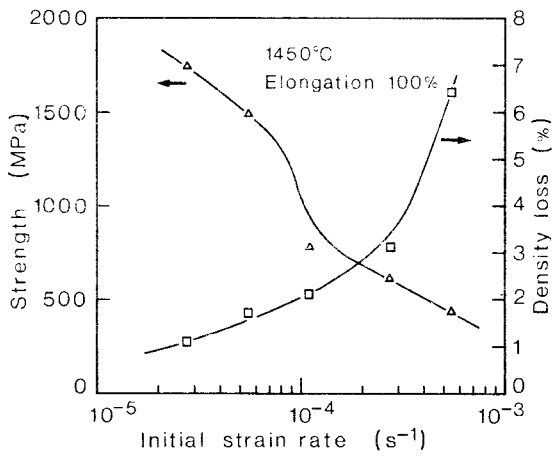

Fig. 9. Density loss and strength after 100% elongation at 1450°C as a function of initial strain rate.

perplastic flow was studied by comparing the grain size in the deformed (dynamic annealing) section with that in the undeformed (static annealing) one within the same elongated specimen.[24,25] The average grain size of elongated grains is defined by the following equation:

$$d = (d_1 \cdot d_2)^{1/2} \tag{4}$$

The relative increase of grain size is defined as $\Delta d/d_0$, where Δd is the difference between the grain size of the annealed specimen and the initial grain size, d_0. The $\Delta d/d_0$ value is plotted as a function of time in Fig. 8. The result clearly shows enhanced grain growth during dynamic annealing compared with grain growth during static annealing. The grain growth of Al_2O_3 was less than that of ZrO_2. Since many Al_2O_3 grains were dispersed and isolated in the ZrO_2 matrix, diffusion of Al^{3+} through ZrO_2 grains was required for grain coarsening of Al_2O_3. On the other hand, coarsening ZrO_2 grains which were connected with each other occurred more easily by elimination of ZrO_2-ZrO_2 boundaries.

Cavity formation occurred in superplastically elongated specimens (Fig. 7(*B*) and (*C*)). The density of cavity distribution and cavity size was dependent on the strain rate, both decreasing with decreasing strain rate. Cavitation was quantitatively evaluated by measuring density loss of the deformed material. The density loss and the strength of specimens which were deformed to a constant strain (100%) at various strain rates are shown in Fig. 9. The effect of strain rate on cavitation may be divided into two regions. In the low-strain-rate region ($<10^{-4}$ s^{-1}), the density loss decreased linearly in proportion to the logarithm of strain rate. At higher strain rates ($>10^{-4}$ s^{-1}), the density loss increased rapidly.

The strength of deformed specimens is the measure of cavitation damage. Generally, the strength of elongated specimens (100%) decreased with the increase of strain rate. At higher strain rates ($>10^{-4}$ s^{-1}), the strength degradation was severe. However at lower strain rates, the specimens maintained a strength of ≧1500 MPa. Recently Masaki and Murata[26] reported that TZP containing 2.5 mol% Y_2O_3 (100% tetragonal grains) changed its microstructure after aging at 1200°C for 1000 h, forming repeated twin structures within the grains. The crystalline phase of superplastically deformed Y-TZP was examined by X-ray diffractometry (XRD), but monoclinic lines were not detected.[9] The XRD result suggested that tetragonal ZrO_2 grains in a specimen which was exposed to high temperatures for a relatively short period did not transform into monoclinic grains. Therefore, the strength degradation of elongated specimens was considered to be caused not by phase change but by cavity formation or creep crack growth.

The creep crack growth perpendicular to the direction of tensile stress was observed on the surface of as-deformed specimens elongated at strain rates higher than 5×10^{-4} s^{-1} (Fig. 10(*A*)). In the specimens deformed at lower strain rates, small voids were formed on the surface, but they did not develop into creep cracks (Fig. 10(*B*)).

DISCUSSION

RHEOLOGICAL NATURE OF THE COMPOSITE

The TZP/Al_2O_3 material is a composite in which the second phase, Al_2O_3 grains, are uniformly dispersed among fine ZrO_2 grains. The material contained 20 wt% Al_2O_3 grains which corresponded to a volume fraction of 28%. In the composite, the flow behavior of the TZP matrix may be modified by the second-phase particles. The constitutive equation for the superplastic Y-TZP could be described by Eq. (3), where $n = 2$ and $p = 2$. The activation energy value (600 kJ/mol) was larger than that of the lattice diffusion constant of cations or anions.[7] The broken line in Fig. 5 represents the flow stress-strain rate relation reported previously for Y-TZP at 1350°C.[8] Because the grain size of Y-TZP was different from that of the composite, the flow stress of Y-TZP shown in Fig. 5 was corrected correspondingly to the grain size of deformed composite (0.65 μm) according to Eq. (3). There was fair agreement in the value of stress exponent between the composite and Y-TZP, but the flow resistance of the composite was higher than that of Y-TZP. A similar correction concerning the grain size of Y-TZP was carried out on the strain rate and plotted as a function of reciprocal of temperature in Fig. 6. The slope of the broken line representing the activation energy of Y-TZP approximately corresponded to that of the composite, but the strain rate of the composite was less than that of Y-TZP.

As Al_2O_3 grains are randomly dispersed and surrounded by ZrO_2 grains, the deformation of the composite is rather similar to the flow of a non-Newtonian fluid containing a significant volume fraction of second-phase particles.[27,28] The non-Newtonian flow of the matrix may be expressed as follows:

$$\dot{\varepsilon} = \alpha\sigma^n \qquad \text{(Norton equation)} \tag{5}$$

Chen[28] showed that the solutions of non-Newtonian flow of a fluid mixture containing a volume fraction (ρ) of spherical inclusions dispersed in a matrix which obeys a flow relation given by Eq. (5), are:

$$\dot{\varepsilon} = (1 - \rho)^{2+n/2}\alpha\sigma^n \qquad \text{(hard inclusions)} \tag{6}$$

and

$$\dot{\varepsilon} = (1 - \rho)^{-(53n+7)/36}\alpha\sigma^n \qquad \text{(soft inclusions)} \tag{7}$$

Chen's[28] rheological considerations predicted that the constitutive equation of a non-Newtonian material containing the second phase which had different deformation properties from those of the matrix should follow the same Norton law as that of matrix but have a numerical factor proportional to $(1 - \rho)^q$, where q is an exponent as given by Eq. (6). The observed similarities in the

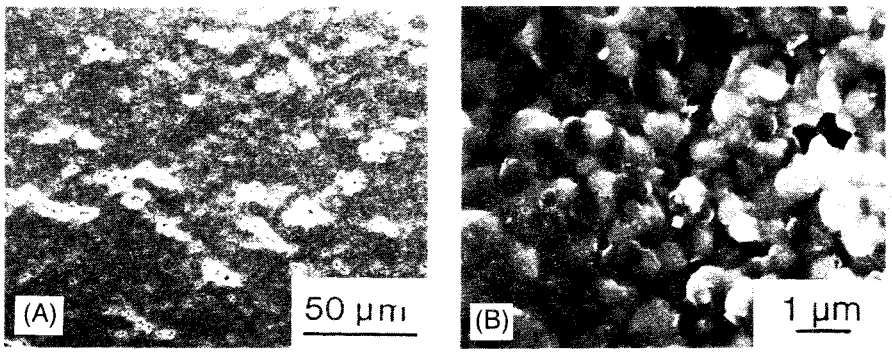

Fig. 10. Micrographs of surface of elongated (at 1450°C) specimen (tension axis is vertical) (*A*) $\dot{\varepsilon}_0 = 5.56 \times 10^{-4}\ s^{-1}$, 107% (the region near the fracture tip) and (*B*) $\dot{\varepsilon}_0 = 2.78 \times 10^{-4}\ s^{-1}$, 158%.

superplastic behavior of Y-TZP and TZP/Al_2O_3 composite can be interpreted using this analysis. In TZP/Al_2O_3 composite, the presence of the second-phase Al_2O_3 grains affected superplastic flow, so that the strain rate was lowered. The elastic constants of Al_2O_3 and that of ZrO_2 at 1400°C were 280 and 100 GPa, respectively.[29] In this sense, Al_2O_3 grain is "harder" than ZrO_2 grain. By assuming $n = 2$ in Eq. (6), the volume fractions of the hard second phase were inferred to be from 22 to 26% to account for the reduction of the observed strain rates of the composite from that of TZP. The nominal volume fraction (28%) of Al_2O_3 grains agreed well with the calculated value.

The deformation behavior of ZrO_2-based composite containing Al_2O_3 grains could be interpreted as non-Newtonian flow containing incompressible particles. From a rheological point of view, the superplastic flow can be expected in a wide spectrum of ZTC containing harder grains than Al_2O_3. Accordingly, toughened ZrO_2 ceramics with equiaxed fine mullite, SiC, or Si_3N_4 grain dispersions are assumed to show superplasticity if cavity formation or creep crack growth can be avoided during deformation.

Measurement of grain elongation has shown that grain-boundary sliding is the predominant mechanism of superplastic flow in Y-TZP and TZP/Al_2O_3 composites. Several mechanisms for local accommodation mechanisms at triple points for the grain-boundary sliding may involve both diffusion processes and dislocation activity at the grain boundary. Sherby *et al.*[3] developed a phenomenological equation for a large number of superplastic metals:

$$\dot{\varepsilon} = 2 \times 10^9 D_{eff}/d^2(\sigma/E)^2 \qquad (8)$$

where D_{eff} is the effective diffusion coefficient and E is Young's modulus. When lattice diffusion is the rate-controlling process, the creep rate is given by substituting D_L for D_{eff} in Eq. (8), where D_L is the lattice-diffusion coefficient. Equation (8) also fits with experimental data of superplastic flow in Y-TZP within a factor of 2 by substituting the cationic diffusion coefficient for D_{eff}. Although a physical model is not presented, it seems that the empirical GBS Eq. (8) holds true not only for superplasticity in metals but also for superplasticity in ionic polycrystals.

Although the activation energy of the composite was ≈600 kJ/mol, the activation energy of the cation lattice diffusion was 439 kJ/mol[7] and 577 kJ/mol[5] in cubic ZrO_2 (c-ZrO_2) and Al_2O_3, respectively. The diffusion data in tetragonal ZrO_2 (t-ZrO_2) have not been obtained. Since the composite contains t-ZrO_2, c-ZrO_2, and Al_2O_3 grains, the effective diffusion coefficient of the composite may be expressed by a complicated function of diffusion coefficients for these phases. In short, diffusion data from c-ZrO_2 cannot be confidently applied to the composite.

A glassy grain-boundary phase has been frequently observed in TZP and TZP/Al_2O_3 composites by many researchers.[30,31] Drennan *et al.*[32] reported that the grain-boundary phase appeared to accumulate predominantly at Al_2O_3-ZrO_2 interfaces. If there are glassy layers, grain-boundary sliding may be promoted, but the rate-controlling process may be the accommodation at triple points. The value of the observed stress exponent, 2, excluded the diffusional mechanism of deformation by the solution-reprecipitation process[33] for the TZP and TZP/Al_2O_3 composites.

CAVITY, CREEP CRACK GROWTH, AND FRACTURE

Cavity or void formation is a common phenomenon accompanying superplastic deformation in some materials.[34] For this TZP/Al_2O_3 composite, the density loss during deformation (Fig. 11) indicated that the volume fraction of cavities increased with strain. There are two possible mechanisms for cavity growth,[34] a diffusion-controlled mechanism and a plasticity-controlled one. The diffusional cavity growth occurs due to vacancy diffusion, and the plasticity controlled cavity growth is related to dislocation creep and grain-boundary slid ng. The dominant cavity growth mechanism depends on the radius of void with the plasticity mechanism predominating for larger cavities. The observed cavity size was dependent on strain and strain rate, and it increased with strain rate.

Cavities link and coalesce to form cracks that may finally lead to fracture. The density loss at fracture was also plotted in Fig. 3, with the elongation at failure, as a function of strain rate. The fracture criterion of the superplastic TZP/Al_2O_3 composite is not clear, but it seems that the mode of fracture can be divided into three regions according to the strain rate. There was almost no density loss in the specimen that failed at the highest strain rate and at the highest stress. The creep crack growth of the preexisted flaw caused fracture at this region. In the intermediate strain rate from $5 \times 10^{-4}\ s^{-1}$ to $5 \times 10^{-3}\ s^{-1}$, fracture occurred with a density loss of ≈6%, suggesting the cavity-growth-controlled fracture. The overall cavitation and accompanied creep cracks were observed on the surface of the specimens.

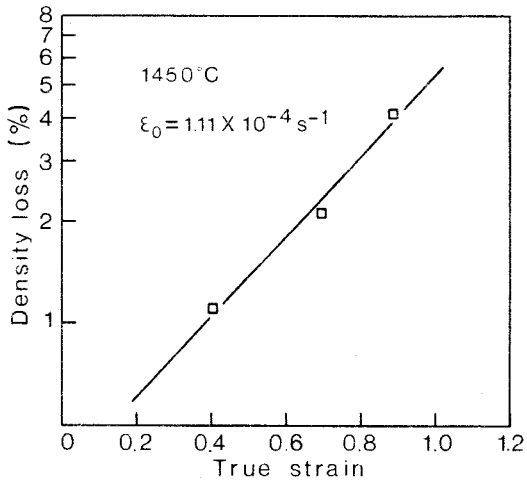

Fig. 11. Increase in cavity volume fraction with strain.

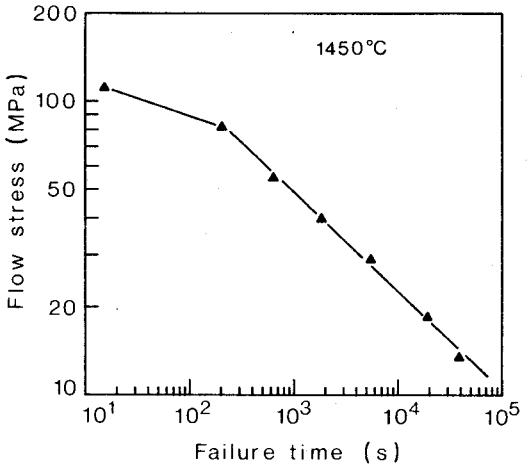

Fig. 12. Failure time plotted as a function of nominal stress.

At the lowest strain rate region, specimens fractured at an elongation of 200% with the density loss of ≈2.7%. Slight non-uniform deformation was observed only in the vicinity of the fracture surface. Namely, the diameter of the specimen (original diameter of 3 mm) became 1.40 mm at the fracture tip, and the diameter at the middle of the gage length was 1.75 mm. Creep cracks were not observed except for the fracture tip. The length of the uniform temperature region in the furnace was ≈50 mm. The maximum elongation was dependent on the gage length of the tensile specimen so that the elongation of 200% was achieved by using a specimen with a gage length of 16 mm, but the elongation was limited to 160% by using a specimen with a gage length of 30 mm. So it was concluded that the length of the homogeneous temperature region in the furnace was one factor that limited the maximum elongation.

The elongation vs strain-rate diagram is converted and re-plotted in flow stress vs time to failure (t_f) diagram (Fig. 12). It seems that the failure time can be expressed as a function of nominal flow stress:

$$\ln (t_f) = \ln B - n^* \ln \sigma \tag{9}$$

where B is a constant and n^* is obtained from the slope of the $\sigma - t_f$ relation. The failure time in the cavity growth-controlled region was characterized by $n^* = 3$. Under uniform temperature distribution, unstable deformation can be avoided, so that the maximum strain would be expressed in the following equation from Eqs. (5) and (9):

$$\begin{aligned} \varepsilon_{max} &= \varepsilon t_f \\ &= \alpha B \sigma^{n-n^*} \\ &\approx \alpha B/\sigma \end{aligned} \tag{10}$$

As a result, an elongation of >400% can be expected for a composite under ideal testing conditions.

The effect of cavitation damage or creep crack growth can be reduced by keeping the strain rate sufficiently slow. Therefore the strength degradation caused by superplastic forming can be avoided, as is demonstrated by the fact that an elongated specimen (100%) maintained a room-temperature strength of 1800 MPa.

CONCLUSION

The two-phase TZP/Al_2O_3 composite exhibited superplasticity in uniaxial tension. Elongation of >200% occurred at slow strain rates, but elongation decreased with increasing strain rate.

The temperature and stress dependence of superplasticity in the composite followed the constitutive equation of Y-TZP. The superplastic rheological behavior of the composite appears to be similar to that of non-Newtonian fluid containing the second-phase particles.

Failures in superplasticity occurred by cavitation and creep crack growth. Cavity growth was suppressed at slow strain rates, and cavitation damage could be avoided or minimized by controlling the strain rate.

ACKNOWLEDGMENTS

The authors would like to thank Prof. N. Soga of Kyoto University and Dr. K. Hayakawa for their kind discussions. Our colleagues, S. Sakaguchi and N. Murayama, are acknowledged for their cooperation.

REFERENCES

[1]J. W. Edington, K. N. Melton, and C. P. Cutler, "Superplasticity," *Prog. Mater. Sci.*, **21**, 61–170 (1976).
[2]J.-G. Wang and R. Raj, "Mechanism of Superplastic Flow in a Fine-Grained Ceramic Containing Some Liquid Phase," *J. Am. Ceram. Soc.*, **67** [6] 399–409 (1984).
[3]O. D. Sherby, R. D. Caligiuri, E. S. Kayali, and R. A. White; pp. 1–39 in Advances in Metal Processing. Edited by J. J. Burk, R. Mehrabian, and V. Weiss. Plenum, New York, 1981.
[4]A. G. Evans, J. R. Rice, and J. P. Hirth, "Suppression of Cavity Formation in Ceramics: Prospects for Superplasticity," *J. Am. Ceram. Soc.*, **63** [7–8] 368–75 (1980).
[5]K. R. Venkatachari and R. Raj, "Superplastic Flow in Fine-Grained Alumina," *ibid.*, **69** [2] 135–38 (1986).
[6]C. Carry and A. Mocellin; pp. 16.1–16.19 in Superplasticity. Edited by B. Baudelet and M. Suery. Edition du CNRS, 1985.
[7]F. Wakai, S. Sakaguchi, and Y. Matsuno, "Superplasticity of Yttria-Stabilized Tetragonal ZrO_2 Polycrystals," *Adv. Ceram. Mater.*, **1** [3] 259–63 (1986).
[8]F. Wakai, S. Sakaguchi, N. Murayama, H. Kato, and K. Kuroda; to be published in Advances in Ceramics, Science and Technology of Zirconia III.
[9]F. Wakai, S. Sakaguchi, K. Kanayama, H. Kato, and H. Onishi; pp. 315–22 in Ceramic Materials and Components for Engines. Edited by W. Bunk and H. Hausner. Deutsche Keramische Gesellschaft, 1986.
[10]C. Carry and A. Mocellin; p. 1043 in High Tech Ceramics. Edited by P. Vincenzini. Elsevier, 1987.
[11]F. F. Lange, "Transformation-Toughened ZrO_2: Correlations between Grain Size Control and Composition in the System ZrO_2-Y_2O_3," *J. Am. Ceram. Soc.*, **69** [3] 240–42 (1986).
[12]F. F. Lange and M. M. Hirlinger, "Hindrance of Grain Growth in Al_2O_3 by ZrO_2 Inclusions," *ibid.*, **67** [3] 164–68 (1984).
[13]B. J. Kellett and F. F. Lange, "Hot Forging Characteristics of Fine-Grained ZrO_2 and Al_2O_3/ZrO_2 Ceramics," *ibid.*, **69** [8] C-172–C-173 (1986).
[14]B. J. Kellett and F. F. Lange, "Hot Forging Characteristics of Transformation Toughened Al_2O_3/ZrO_2 Composite; to be published in *J. Mater. Research.*
[15]F. Wakai, H. Kato, S. Sakaguchi, and N. Murayama, "Compressive Deformation of Y_2O_3-Stabilized ZrO_2/Al_2O_3 Composite," *J. Ceram. Soc. Jpn. (Yogyo-Kyokai-Shi)*, **94** [9] 1017–20 (1986).
[16]K. Tsukuma, K. Ueda, and M. Shimada, "Strength and Fracture Toughness of Isostatically Hot-Pressed Composites of Al_2O_3 and Y_2O_3-Partially Stabilized ZrO_2," *J. Am. Ceram. Soc.*, **68** [1] C-4–C-5 (1985).
[17]K. Tsukuma, K. Ueda, K. Matsushita, and M. Shimada, "High-Temperature Strength and Fracture Toughness of Y_2O_3-Partially Stabilized ZrO_2/Al_2O_3 Composites," *ibid.*, **68** [2] C-56–C-58 (1985).
[18]F. Wakai, S. Sakaguchi, Y. Matsuno, and H. Okuda; pp. 279–85 in Proc. 1st Int'l. Symp. on Ceramic Components for Engines. Edited by S. Somiya, E. Kanai, and K. Ando. KTK Scientific, Tokyo, and D. Reidel, Boston, 1984.
[19]T. Oji, S. Sakai, M. Ito, Y. Yamauchi, W. Kanematsu, and S. Ito, "Tensile Strength of HP-Si_3N_4 at Room and Elevated Temperatures," *J. Ceram. Soc. Jpn. (Yogyo-Kyokai-Shi)*, **94** [10] 1056–61 (1986).
[20]J. J. Jonas; pp. 57–68 in Superplastic Forming of Structural Alloys. Edited by N. E. Paton and C. H. Hamilton. Metallurgical Soc. of AIME, 1982.
[21]T. G. Langdon; pp. 27–40 in Superplastic Forming of Structural Alloys. Edited by N. E. Paton and C. H. Hamilton. Metallurgical Soc. of AIME, 1982.
[22]A. H. Heuer, N. J. Tighe, and R. M. Cannon, "Plastic Deformation of Fine-Grained Alumina (Al_2O_3): II, Basal Slip and Nonaccommodated Grain-Boundary Sliding," *J. Am. Ceram. Soc.*, **63** [1–2] 53–58 (1980).
[23]A. Dominguez-Rodriguez, K. P. D. Lagerof, and A. H. Heuer, "Plastic Deformation and Solid-Solution Hardening of Y_2O_3-Stabilized ZrO_2," *ibid.*, **69** [3] 281–84 (1986).
[24]B. Kashyap, A. Arieli, and A. K. Mukherjee, "Review: Microstructural Aspects of Superplasticity," *J. Mater. Sci.*, **20**, 2661–86 (1985).
[25]M. A. Clark and T. H. Alden, "Deformation Enhanced Grain Growth in a Superplastic Sn-1% Bi Alloy," *Acta Metall.*, **21**, 1195–1206 (1973).
[26]T. Masaki and Y. Murata, "Microstructure of Y-PSZ after Aging at High Temperature," *J. Mater. Sci.*, **22**, 407–14 (1987).
[27]M. Suery and B. Baudelet, "Hydrodynamical Behavior of a Two-Phase Superplastic Alloy: α/β Brass," *Philos. Mag.* A, **41** [1] 41–64 (1980).
[28]I.-Wei Chen; 5.1–5.20 in Superplasticity. Edited by B. Baudelet and M. Suery. Edition du CNRS, 1985.
[29]J. B. Wachtmann, Jr. and D. G. Lam, Jr, "Young's Modulus of Various Refractory Materials as a Function of Temperature," *J. Am. Ceram. Soc.*, **42** [5] 254–60 (1959).
[30]M. Rühle, N. Claussen, and A. H. Heuer; pp. 352–70 in Advances in Ceramics, Vol. 12. Edited by N. Claussen, M. Rühle, and A. H. Heuer. American Ceramic Society, Columbus OH, 1985.
[31]B. Kibbel and A. H. Heuer, "Exaggerated Grain Growth in ZrO_2-Toughened Al_2O_3," *J. Am. Ceram. Soc.*, **69** [3] 231–36 (1986).
[32]J. Drennan, S. P. S. Badwal, and V. Gross, "The Influence of Al_2O_3 Additions to Yttria Containing Tetragonal Zirconia Polycrystals (Y-TZP): A Microstructural and Electrical Conductivity Study"; to be published in Advances in Ceramics, Science and Technology of Zirconia III.
[33]R. Raj, R. L. Tsai, J.-G. Wang, and C. K. Chyung; pp. 353–78 in Deformation of Ceramic Materials II. Edited by R. E. Tressler and R. C. Bradt. Plenum, New York, 1984.
[34]M. J. Stowell; pp. 321–36 in Superplastic Forming of Structural Alloys. Edited by N. E. Paton and C. H. Hamilton. Metallurgical Soc. of AIME, 1982.